Digital Camera Zooming Based on Unified CFA Image Processing Steps

R. Lukac, K. Martin, and K.N. Plataniotis

Abstract — *A unified camera image processing system that performs zooming and full color image reconstruction for single-sensor digital cameras is introduced. Compact and low-cost single-sensor solutions often lack optical zooming capabilities and thus depend on digital techniques. However, the computational power required for high-quality output using traditional techniques is generally too prohibitive to implement in such devices. The proposed scheme employs a small number of reusable, low-complexity operations and a consistent color model throughout to achieve high-quality zoomed output that is practical for hardware implementation. The high-level system components are color filter array (CFA) zooming, CFA interpolation (demosaicking) and demosaicked image postprocessing. The resulting output is consistently superior to other methods.* [1]

Index Terms — Camera image processing, Bayer pattern, color filter array interpolation, color image restoration, image zooming, demosaicked image postprocessing.

I. INTRODUCTION

In recent times, single-sensor digital cameras (Fig. 1) have become commonplace as consumers choose the convenience they offer over traditional film photography. However, the sensor, typically a charge coupled device (CCD) or a complementary metal-oxide semiconductor (CMOS), is essentially a monochromatic device being only capable of obtaining a single measurement of luminance per spatial location. To overcome this limitation, a color filter array (CFA) is used to separate incoming light into a specific spatial arrangement of color components. The Bayer pattern shown in Fig. 2 [1] is the most common CFA, providing a mosaic of Red (R), Green (G), and Blue (B) color components.

Technological advances have allowed for the miniaturization of these single-sensor cameras [2],[3], resulting in their being embedded in a myriad of consumer electronic devices. Many of these devices, such as mobile phones and personal digital assistants (PDAs), are restricted in their optical capabilities and computational resources and thus provide limited functionality and quality of output. Specifically, zooming functionality, if present, is usually augmented or performed solely using digital interpolation *after*

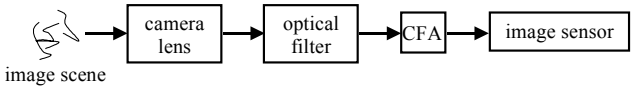

Fig. 1. A single-sensor architecture.

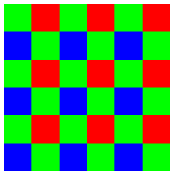

Fig. 2. Bayer CFA pattern.

demosaicking of the Bayer pattern image into a full color image [3],[4]. The lack of sharpness and false color artifacts commonly present in demosaicked images are thus amplified. Also, the computational and memory requirements of full color interpolation make it prohibitive for hardware implementation.

In this paper, we introduce a cost-effective digital zooming solution for single-sensor digital cameras. The proposed method performs the CFA zooming, CFA interpolation (demosaicking) and demosaicked image postprocessing operations using local color ratios and edge-sensing weight coefficients utilized in each above sub-procedure. This unifies all the algorithmic steps into a unique digital image zooming framework useful for cost-effective hardware implementations in single-sensor cameras. The employed edge-sensing mechanism tracks varying image statistics, whereas the use of local color ratios avoids to output color artifacts. Therefore, the unified framework produces the enlarged, full color camera output as a sharp, visually pleasing color image.

The paper is organized as follows: Section II describes the unified camera image processing system in detail; Section III presents the experimental results; and the paper concludes in Section IV.

II. UNIFIED CAMERA IMAGE PROCESSING SYSTEM

Let us consider, a $K_1 \times K_2$ Bayer CFA image $\mathbf{b}(i): Z^2 \to Z^3$ representing a two-dimensional matrix of three-component RGB vectors:

$$\mathbf{b}_{(m,n)} = \begin{cases} (b_{(m,n)1}, 0, 0) & \text{for (odd } m\text{, even } n\text{)}, \\ (0, 0, b_{(m,n)3}) & \text{for (even } m\text{, odd } n\text{)}, \\ (0, b_{(m,n)2}, 0) & \text{otherwise.} \end{cases} \quad (1)$$

where (m,n), for $m = 1,2,...,K_1$ and $n = 1,2,...,K_2$, denotes the spatial position of the incomplete RGB vector

[1] Manuscript received November 13, 2003.

The authors are with The Edward S. Rogers Sr. Department of ECE, University of Toronto, Toronto, Canada.

Corresponding Author: Dr. Rastislav Lukac, Bell Canada Multimedia Laboratory, Room BA 4157, The Edward S. Rogers Sr. Department of ECE, University of Toronto, 10 King's College Road, Toronto, Ontario, M5S 3G4, Canada (e-mail: lukacr@ieee.org)

Contributed Paper
Manuscript received November 24, 2003

$\mathbf{b}_{(m,n)} = (b_{(m,n)1}, b_{(m,n)2}, b_{(m,n)3})$ with only one available color component $b_{(m,n)k}$, for $k = 1,2,3$. Based on the Bayer CFA pattern structure, R components $b_{(m,n)1}$ are located at $(\text{odd } m, \text{even } n)$, and B components $b_{(m,n)3}$ are located at $(\text{even } m, \text{odd } n)$. The rest of locations in the Bayer image $\mathbf{b}(i)$ correspond to the G components $b_{(m,n)2}$.

The proposed unified camera image processing system is comprised of three distinct, yet interconnected, components: a) CFA zooming to generate a higher resolution Bayer CFA image from the original CFA data; b) CFA interpolation to generate a full color image from the higher resolution CFA image and c) postprocessing to reduce distracting artifacts and enhance sharpness in the final output.

Key to the unified system is the required implementation of only a small number of basic, low-complexity operations. These operations are used repeatedly in the various system components with varying parameters. This lends itself to efficient hardware implementation.

Another important aspect of the design is the execution of the CFA zooming *before* demosaicking and postprocessing. The significant advantages of this approach are the reduced computational and memory requirements as a result of performing the zooming on a single channel (Bayer pattern) image, and increased image quality from having color interpolation and postprocessing performed on the higher resolution image.

A. CFA Zooming

To zoom the Bayer data and preserve the Bayer pattern structure, the original CFA data should be assigned unique positions which correspond to the Bayer pattern of an enlarged image.

Consider an arbitrary integer zooming factor λ. Assume that $\mathbf{x}(i): Z^2 \to Z^3$ represents a $\lambda K_1 \times \lambda K_2$ Bayer image with increased spatial resolution compared to the original CFA image $\mathbf{b}(i)$. Applying the approach of [4], the original values of $\mathbf{b}(i)$ are filled into the zoomed image $\mathbf{x}(i)$ as follows:

$$\left.\begin{array}{l} \mathbf{x}_{(2m-1,2n)} \\ \mathbf{x}_{(2m,2n-1)} \\ \mathbf{x}_{(2m-1,2n-1)} \end{array}\right\} = \mathbf{b}_{(m,n)} \quad \begin{array}{l} \text{for } (\text{odd } m, \text{even } n) \\ \text{for } (\text{even } m, \text{odd } n) \\ \text{otherwise} \end{array} \tag{2}$$

where (m,n) denotes the coordinates in the original (smaller) Bayer image $\mathbf{b}(i)$ shown in Fig. 2. Fig. 3a shows the zoomed image $\mathbf{x}(i)$ filled in with the original CFA data from $\mathbf{b}(i)$.

Let us consider that (r,s), for $r = 1,2,...,\lambda K_1$ and $s = 1,2,...,\lambda K_2$, denotes the spatial position in the enlarged image $\mathbf{x}(i)$, shown in Fig. 3a, containing only the original Bayer CFA data of $\mathbf{b}(i)$. Missing G components $x_{(r,s)2}$ of $\mathbf{x}(i)$ are generated using a weighted sum of the surrounding original G components $x_{(i,j)2}$ as follows:

$$x_{(r,s)2} = \sum_{(i,j)\in\zeta} w_{(i,j)} x_{(i,j)2}, \tag{3}$$

where (r,s) is the location at the centre of the diamond-shaped structure shown in Fig. 3a. The original G components utilized in the operation are located at $\zeta = \{(r-2,s),(r,s-2),(r,s+2),(r+2,s)\}$. The normalized weights $w_{(i,j)}$ are generated via

$$w_{(i,j)} = u_{(i,j)} / \sum_{(g,h)\in\zeta} u_{(g,h)} \tag{4}$$

where the positive edge-sensing coefficients $u_{(i,j)}$ are defined as follows:

$$u_{(i,j)} = \frac{1}{1 + \sum_{(g,h)\in\zeta} |x_{(i,j)k} - x_{(g,h)k}|}. \tag{5}$$

It has to be mentioned that k in (5) always corresponds to k describing the interpolated component and therefore, $k = 2$ in (3). In (5), the denominator incorporates an aggregate absolute difference between the CFA input located at (i,j) and the rest of the CFA inputs described by ζ. For an outlying value $x_{(i,j)2}$ that is highly dissimilar to the rest of the values, the aggregate distance will approach infinity and $u_{(i,j)}$ will approach zero, thus decreasing the emphasis on $x_{(i,j)2}$ in generating $x_{(r,s)2}$. Alternatively, if $x_{(i,j)2}$ is similar to the other values, $u_{(i,j)}$ will approach a maximum value of unity. This methodology preserves edge features by detecting the trend of the surrounding components.

To complete the remaining missing G components, (3) is repeated with (r,s) located at the centre of the square-shaped structure shown in Fig. 3b. The structure, with $\zeta = \{(r-1,s-1),(r-1,s+1),(r+1,s-1),(r+1,s+1)\}$, incorporates two original G components and two interpolated G components from the previous step. The weights are again calculated using (4) and (5) with $k = 2$ and the square-shaped structure ζ.

To constitute the missing R (and B) components, a local color ratio (LCR) model [5] is employed. For each position that requires the estimation of an R (or B) component, a local R/G (or B/G) ratio is generated using surrounding positions. Since G components are not present in the same locations as the R (or B) components, adjacent surrounding G components with the identical shift on the image lattice are used to create the LCR. The missing R (or B) component at the centre of the surrounding structure is estimated using the surrounding LCR and the G component adjacent to the centre. This takes advantage of the expected relative uniformity of the LCR and the abundance of available green information, which is more accurate due to a twice as frequent occurrence of the original G CFA components compared to the R and B components.

The R components $x_{(r,s)1}$ are obtained as follows:

$$x_{(r,s)1} = x_{(r,s-1)2} \sum_{(i,j)\in\zeta} w_{(i,j)} \{x_{(i,j)1} / x_{(i,j-1)2}\} \tag{6}$$

where (r,s) is the location at the centre of the square-shaped

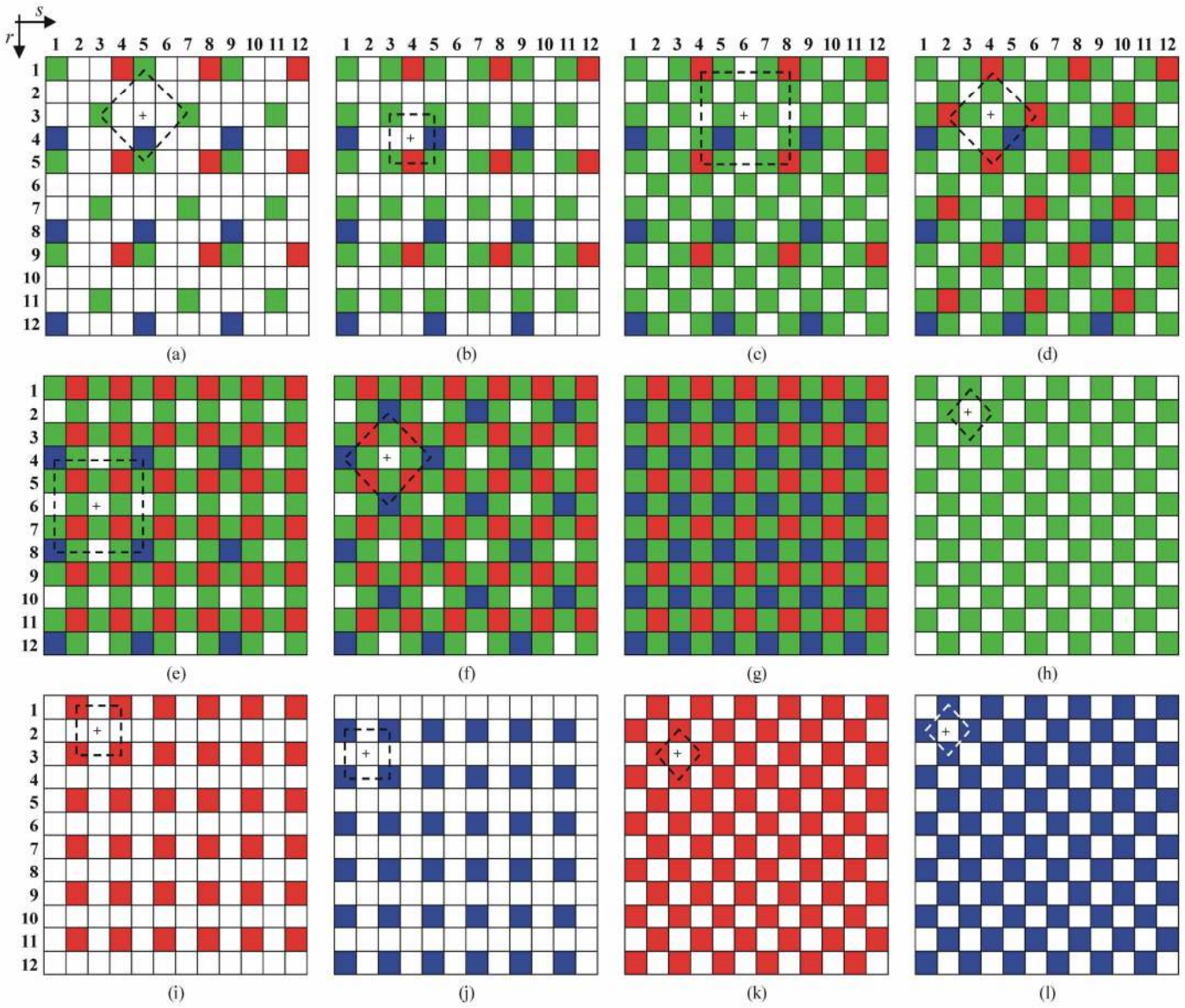

Fig. 3. The spatial arrangements of the CFA components obtained applying the proposed unified image processing steps: (a-g) during CFA zooming, (h-l) during CFA interpolation (demosaicking) and demosaicked image postprocessing.

structure shown in Fig. 3c. The structure is formed by the original R components $x_{(i,j)1}$ positioned at locations $\zeta = \{(r-2,s-2),(r-2,s+2),(r+2,s-2),(r+2,s+2)\}$. The LCR is generated using these original R components $x_{(i,j)1}$ and the adjacent interpolated G components $x_{(i,j-1)2}$ positioned one unit to the left compared to $x_{(i,j)1}$. The missing R component $x_{(r,s)1}$ is estimated using the LCR and the interpolated G component $x_{(r,s-1)2}$ positioned one unit to the left. The coefficient $w_{(i,j)}$ denotes the normalized weights defined in the same manner as in (4) and (5), with $k=1$. As in (3), $w_{(i,j)}$ de-emphasizes extreme colors in order to provide an intelligent LCR model.

The remaining missing R components are generated with another repetition of (6), except with the diamond-shaped structure of both original and interpolated R components located at $\zeta = \{(r-2,s),(r,s-2),(r,s+2),(r+2,s)\}$, as shown in Fig. 3d.

The B components $x_{(r,s)3}$ are generated in a similar manner as follows:

$$x_{(r,s)3} = x_{(r-1,s)2} \sum_{(i,j)\in\zeta} w_{(i,j)} \{x_{(i,j)3} / x_{(i-1,j)2}\}, \quad (7)$$

where $\zeta = \{(r-2,s-2),(r-2,s+2),(r+2,s-2),(r+2,s+2)\}$ denotes the positions of the original B components $x_{(i,j)3}$ in the square-shaped structure shown in Fig. 3e. The weights are generated using (4) and (5) with $k=3$. The G components $x_{(i-1,j)2}$, positioned one unit downward, are used in conjunction with the original B components $x_{(i,j)3}$ to generate the LCR. The remaining B components are again generated with (7), based on the diamond structure (Fig. 3f) using $\zeta = \{(r-2,s),(r,s-2),(r,s+2),(r+2,s)\}$.

Upon completion of this step, the enlarged Bayer pattern shown in Fig. 3g is obtained.

B. CFA Interpolation

The proposed unified camera image processing system continues by interpolating the enlarged Bayer pattern image into a full color image. This step is unified with the previous CFA zooming step in that the same weighting and LCR model is utilized to estimate the missing R and B color components.

As such, the missing G ($k = 2$) components are estimated using (3)-(5) with the diamond-shaped structure $\zeta = \{(r-1,s),(r,s-1),(r,s+1),(r+1,s)\}$ shown in Fig. 3h.

The R ($k = 1$) and B ($k = 3$) components are given by

$$x_{(r,s)k} = x_{(r,s)2} \sum_{(i,j)\in\zeta} w_{(i,j)} \{x_{(i,j)k} / x_{(i,j)2}\} . \quad (8)$$

where $w_{(i,j)}$ are calculated using (4) and (5). It should be noted that (8) is identical to (6) and (7) except that the LCR is generated using G components $x_{(i,j)2}$ in the *same* spatial position as the R or B components $x_{(i,j)k}$. Here, $x_{(r,s)k}$ is located at the centre of the square-shaped structure, as shown in Fig. 3i and Fig. 3j, formed by the CFA components $x_{(i,j)k}$ located at $\zeta = \{(r-1,s-1),(r-1,s+1),(r+1,s-1),(r+1,s+1)\}$. The normalizing G component $x_{(i,j)2}$ used in the LCR is located in the center of ζ.

The remaining missing R and B components are generated using (8) with the diamond-shaped structure $\zeta = \{(r-1,s),(r,s-1),(r,s+1),(r+1,s)\}$ shown in Fig. 3k and Fig. 3l. Once this is completed, a full color image is obtained with each spatial location containing three color components.

C. Postprocessing

The postprocessing operation, the final step in the unified camera image processing system, is employed to reduce false color artifacts and enhance sharpness. It takes advantage of the underlying Bayer pattern present before the CFA interpolation and can be viewed as an iterative update of the components that were estimated during CFA interpolation.

First, the G components estimated during CFA interpolation are updated using an LCR as follows:

$$x_{(r,s)2} = x_{(r,s)k} \sum_{(i,j)\in\zeta} w_{(i,j)} \{x_{(i,j)2} / x_{(i,j)k}\} . \quad (9)$$

If (r,s) is a position which corresponds to a Bayer pattern R component, then $k = 1$ is used. Otherwise the position corresponds to a Bayer pattern B component and $k = 3$. The LCR is generated with the surrounding spatial locations $\zeta = \{(r-1,s),(r,s-1),(r,s+1),(r+1,s)\}$ containing G components $x_{(i,j)2}$ shown in Fig. 3h and restored R ($k = 1$) or B ($k = 3$) components $x_{(i,j)k}$. This is the same operation (8) that was used in the calculation of R and B components for CFA interpolation except that the inverse color ratio is used. The edge-sensing weights $w_{(i,j)}$ used in (9) are calculated based on (4) and (5) with $k = 2$.

The R and B components estimated during CFA interpolation

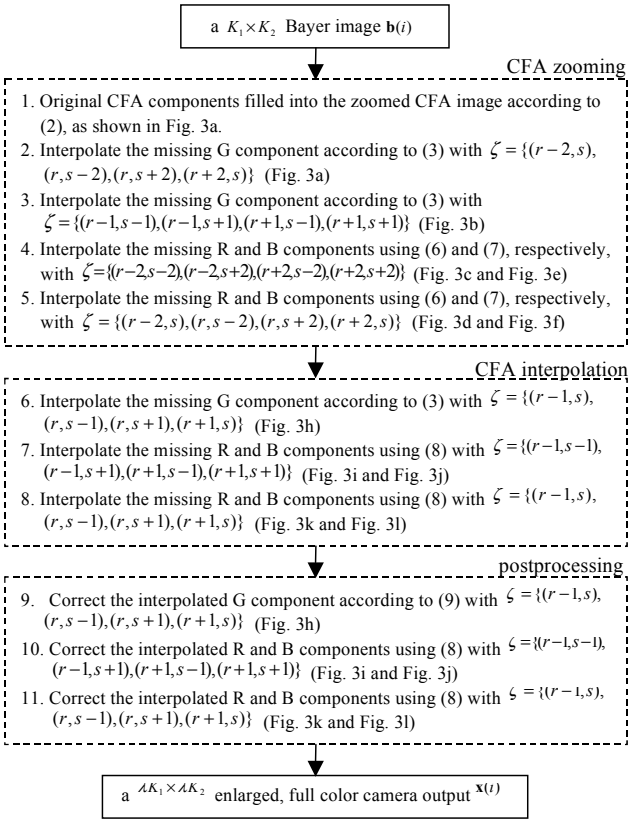

Fig. 4. Block scheme of the proposed unified CFA camera image processing framework with a zooming factor $\lambda = 2$.

are updated in two consecutive steps. First, (8) is used to update R components on Bayer pattern B locations and B components on Bayer pattern R locations. $\zeta = \{(r-1,s-1),(r-1,s+1),(r+1,s-1),(r+1,s+1)\}$, shown in Fig. 3i and Fig. 3j), is used to take advantage of the surrounding Bayer pattern R or B components respectively, along with the previously updated G components in the same positions. Then (8) is repeated in the remaining locations with estimated R or B components using $\zeta = \{(r-1,s),(r,s-1),(r,s+1),(r+1,s)\}$ shown in Fig. 3k and Fig. 3l. For both steps, $w_{(i,j)}$ is calculated using (4) and (5) with either $k = 1$ (updating R) or $k = 3$ (updating B). This completes the correction of all components obtained during CFA interpolation.

Fig. 4 shows a system level diagram of the complete scheme. Each of the three main components is depicted along with references to the formulae required for implementation. Also included are references to the figures describing the structural components within the image that are utilized at various stages.

III. Experimental Results

A number of color images have been used to evaluate the proposed digital zooming framework. Examples are shown in Fig. 5. These images, which have been used extensively in the open literature, have been captured using highly professional three-sensor cameras or color scanners. The images represent natural, real-life scenarios and vary in complexity and color appearance. Note that in order to facilitate comparisons, all

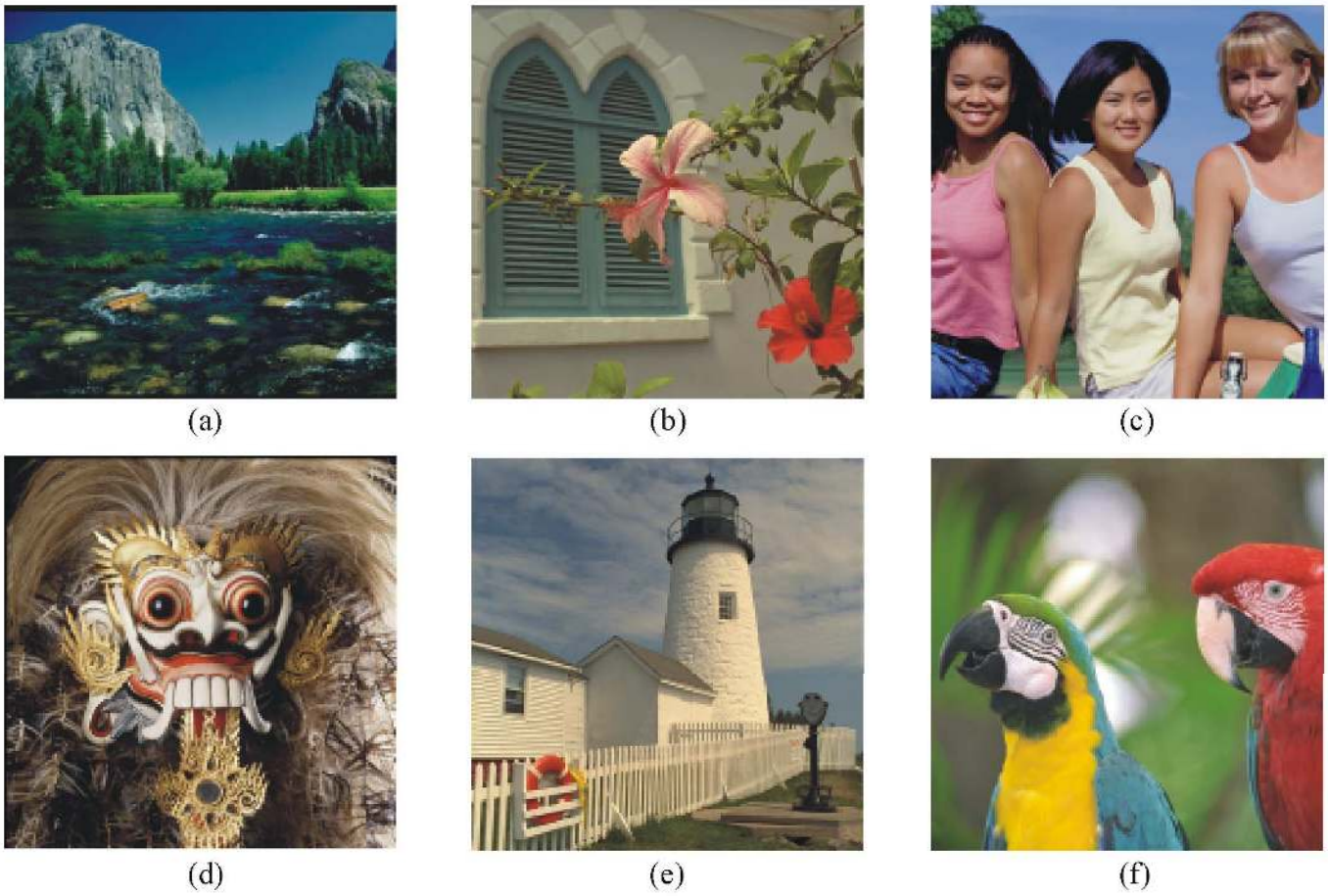

Fig. 5. The test color images: (a) Mountains, (b) Window, (c) Girls, (d) Mask, (e) Lighthouse, (f) Parrots

TABLE I
COMPARISON OF THE METHODS USING THE TEST IMAGE MOUNTAINS

Method	MAE	MSE	NCD
CIZ	10.939	317.0	0.1701
LZ	11.688	362.7	0.1849
CDES	10.478	283.2	0.1879
Proposed unified scheme	10.276	264.2	0.1681

TABLE II
COMPARISON OF THE METHODS USING THE TEST IMAGE WINDOW

Method	MAE	MSE	NCD
CIZ	7.233	155.2	0.0703
LZ	8.288	204.1	0.0908
CDES	6.149	113.4	0.0805
Proposed unified scheme	5.982	104.1	0.0675

TABLE III
COMPARISON OF THE METHODS USING THE TEST IMAGE GIRLS

Method	MAE	MSE	NCD
CIZ	5.839	132.4	0.0730
LZ	6.923	183.2	0.0903
CDES	5.074	100.9	0.0815
Proposed unified scheme	5.191	96.1	0.0764

TABLE IV
COMPARISON OF THE METHODS USING THE TEST IMAGE MASK

Method	MAE	MSE	NCD
CIZ	16.344	623.5	0.1669
LZ	17.736	737.2	0.1879
CDES	14.499	513.6	0.1768
Proposed unified scheme	14.050	463.9	0.1449

TABLE V
COMPARISON OF THE METHODS USING THE TEST IMAGE LIGHTHOUSE

Method	MAE	MSE	NCD
CIZ	9.516	318.7	0.0762
LZ	10.143	362.9	0.0850
CDES	9.118	300.2	0.0674
Proposed unified scheme	9.008	284.8	0.0578

TABLE VI
COMPARISON OF THE METHODS USING THE TEST IMAGE PARROTS

Method	MAE	MSE	NCD
CIZ	4.983	127.6	0.0374
LZ	5.819	158.9	0.0481
CDES	4.608	104.4	0.0413
Proposed unified scheme	4.579	93.2	0.0371

Fig. 6. Zooming steps related to the test image Window: (a) a $\lambda K_1 \times \lambda K_2$ original image $\mathbf{o}(i)$, (b) a $K_1 \times K_2$ down-sampled image $\mathbf{o}_b(i)$, (c) a $K_1 \times K_2$ Bayer image $\mathbf{b}(i)$ used as the started point for the methods, (d) a $\lambda K_1 \times \lambda K_2$ color image obtained by CIZ scheme, (e) a $\lambda K_1 \times \lambda K_2$ color image obtained by the proposed unified scheme.

images have been normalized to the standard 8-bit per channel RGB representation. Since an original Bayer image is unavailable, the evaluation approach follows the steps shown in Fig. 5 or Fig. 6. A $\lambda K_1 \times \lambda K_2$ original color image $\mathbf{o}(i)$ is down-sampled to a $K_1 \times K_2$ color image $\mathbf{o}_b(i)$. This image is sampled with the Bayer CFA pattern in order to obtain a $K_1 \times K_2$ test Bayer image $\mathbf{b}(i)$ used as a starting point for testing purposes [4]-[6]. The proposed unified zooming framework is evaluated by applying it to $\mathbf{b}(i)$. The enlarged camera output $\mathbf{x}(i)$ with size $\lambda K_1 \times \lambda K_2$ obtained using the proposed scheme is compared to the zoomed images achieved by a conventional color image zooming (CIZ) approach (bilinear CFA interpolation [6],[7] followed by bilinear image zooming in the RGB color domain), as well as CFA zooming schemes (CFA zooming followed by bilinear CFA interpolation) such as replication based local CFA zooming (LZ) approach [3] and color-difference edge-sensing CFA zooming (CDES) scheme [4].

Fig. 7. Zooming steps related to the test image Girls: (a) a $\lambda K_1 \times \lambda K_2$ original image $\mathbf{o}(i)$, (b) a $K_1 \times K_2$ down-sampled image $\mathbf{o}_b(i)$, (c) a $K_1 \times K_2$ Bayer image $\mathbf{b}(i)$ used as the started point for the methods, (d) a $\lambda K_1 \times \lambda K_2$ color image obtained by CIZ scheme, (e) a $\lambda K_1 \times \lambda K_2$ color image obtained by the proposed unified scheme.

The performance of the methods is measured, objectively [4], via the mean absolute error (MAE), the mean square error (MSE) and the normalized color difference criterion (NCD).

The objective results are summarized in Tables I-VI and subjective comparison are illustrated in Figs. 6-9. The objective results are included for the sake of completeness; however, the nature of these measures is that they are not efficient in reflecting very localized distortion effects. Consequently, the subjective results are more important here since the goal is to produce visually pleasing output. Given that, for almost all of the twenty test images the proposed unified scheme significantly outperforms all the other schemes in terms of the objective criteria as well as the subjective comparisons.

Fig. 6 and Fig. 7 show examples of final output using CIZ (Fig. 6d) compared with the proposed scheme (Fig. 6e). It can be seen that the proposed scheme exhibits sharper details and avoids the artifacts present along high-contrast edges when

Fig. 8. The selected portion of the results achieved using the test image Mountains (left column), Window (middle column) and Girls (right column) and the following method: (a) original image, (b) CIZ scheme, (c) LZ scheme, (d) CDES scheme, (e) proposed unified scheme.

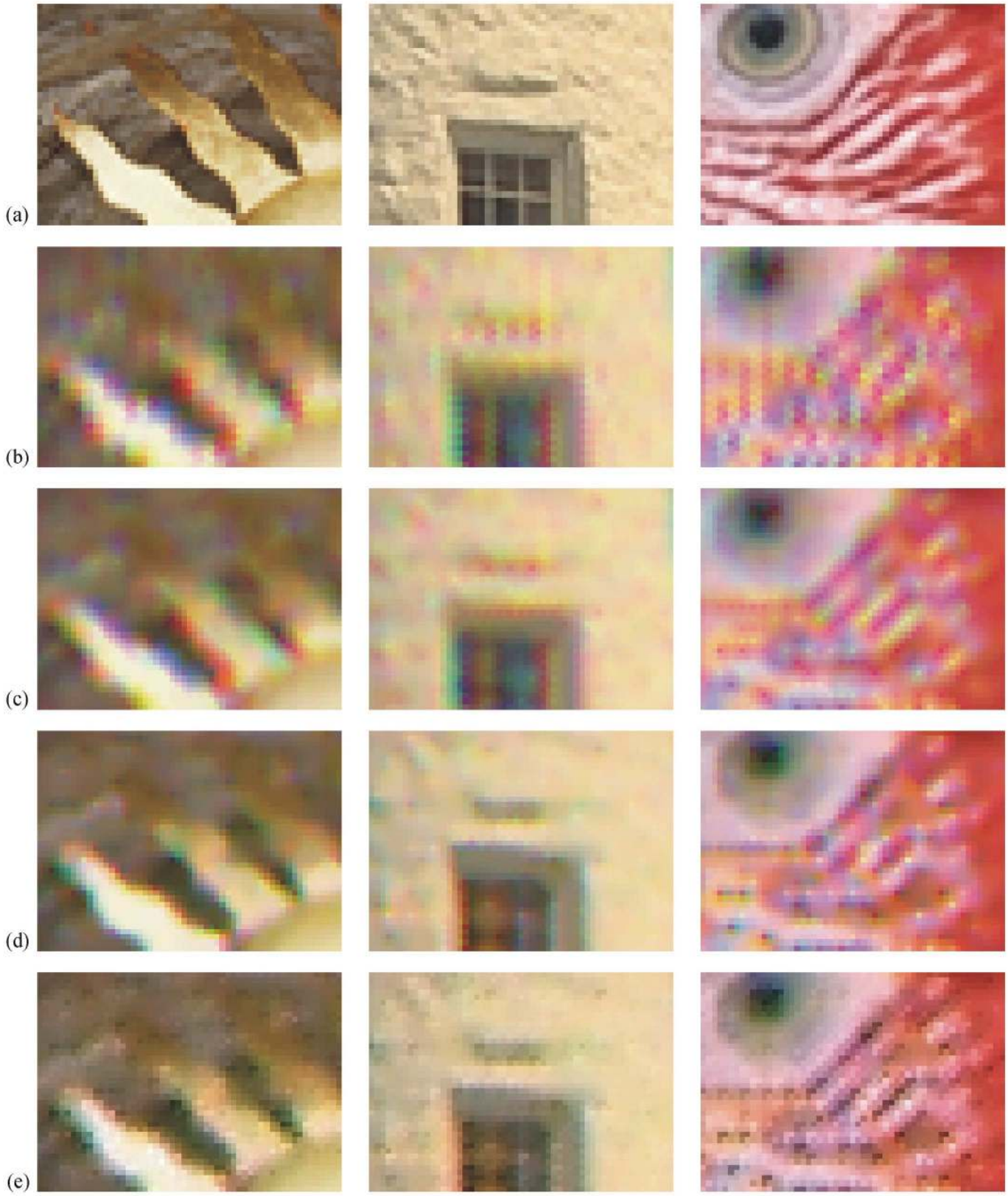

Fig. 9. The selected portion of the results achieved using the test image Mask (left column), Lighthouse (middle column) and Parrots (right column) and the following method: (a) original image, (b) CIZ scheme, (c) LZ scheme, (d) CDES scheme, (e) proposed unified scheme.

using CIZ. The results using the proposed scheme are significantly more visually pleasing.

The most difficult features to handle in CFA zooming and demosaicking are sharp, high contrast edges. In such situations, blurred edges and false color artifacts are the most common forms of distortion. Fig. 8a and Fig. 9a show detailed portions of the original high-resolution images that exhibit these difficult features. The corresponding portion of the zoomed images output from the various schemes are shown in Fig. 8b-e and Fig. 9b-e. The proposed scheme (Fig. 8e and Fig. 9e) maintains the sharpest results compared to the other schemes. Furthermore, the false color artifacts present in CIZ, and LZ and CDES schemes (Fig. 8b-d, Fig. 9b-d) to a lesser degree, are non-existent when using the proposed scheme. Upon comparison, the coloration resulting from the proposed scheme is much truer to the original.

A distracting 'grating' effect is present in the Window and Girls image using the CIZ scheme (Fig. 8b, second and third column). This effect is mostly suppressed by using LZ (Fig. 8c) or CDES (Fig. 8d), but at the cost of significantly reduced sharpness. Using the proposed scheme, the 'grating' effect is mostly suppressed while edge sharpness is maintained (Fig. 8e).

IV. Conclusion

A unified camera image processing system that performs zooming and full color image reconstruction on Bayer pattern images was presented. The framework consists of three main components (CFA zooming, CFA interpolation, and postprocessing) but only utilizes a small number of low-complexity operations that are reused with different parameters throughout the system. This methodology lends itself to efficient hardware implementation. Also, CFA zooming is performed before interpolation so as to reduce the overall computational complexity. By using a consistent framework, high-quality output is achieved without amplification of distracting artifacts.

The experimental results supported the proposed methodology by producing superior output, both objectively and subjectively, when compared to other schemes. Due to the reuse of basic, low-complexity operations, the high quality output can possibly be achieved from direct hardware implementations in compact, low-cost single-sensor imaging devices in which optical zooming functionality is impractical.

Acknowledgment

The work of the first author is supported by a NATO/NSERC Science award.

References

[1] B.E. Bayer, "Color imaging array," *U.S. Patent 3 971 065*, 1976.

[2] B.S. Hur and M.G. Kang, "High definition color interpolation scheme for progressive scan CCD image sensor," *IEEE Trans. Consumer Electronics*, vol. 47, no. 2, pp. 179-186, Feb. 2001.

[3] S. Battiato, G. Gallo, and F. Stanco, "A locally adaptive zooming algorithm for digital images," *Image and Vision Computing*, vol. 20, no. 11, pp. 805-812, Sep. 2002.

[4] R. Lukac, K.N. Plataniotis, and D. Hatzinakos, "Color image zooming on the Bayer pattern," *IEEE Trans. Circuit and Systems for Video Technology*, submitted.

[5] R. Ramanath, W.E. Snyder, G.L. Bilbro, and W.A. Sander III, "Demosaicking methods for Bayer color arrays," *J. Electronic Imaging*, vol. 11, no. 3, pp. 306-315, Jul. 2002.

[6] P. Longere, Z. Xuemei, P.B. Delahunt, and D.H. Brainard, "Perceptual assessment of demosaicing algorithm performance," *Proceedings of the IEEE*, vol. 90, no. 1, pp. 123-132, Jan. 2002.

[7] T. Sakamoto, C. Nakanishi, and T. Hase, "Software pixel interpolation for digital still cameras suitable for a 32-bit MCU," *IEEE Transactions on Consumer Electronics*, vol. 44, no. 4, pp. 1342-1352, Nov. 1998.

Rastislav Lukac received a Diploma in Telecommunications with honors in 1998 and a Ph.D. in 2001, both at the Technical University of Kosice, Slovak Republic. From February 2001 to August 2002 he was an assistant professor at the Department of Electronics and Multimedia Communications at the Technical University of Kosice. Since August 2002 he is a researcher in Slovak Image Processing Center in Dobsina, Slovak Republic. From January 2003 to March 2003 he was a post-doc at Artificial Intelligence & Information Analysis Lab at the Aristotle University of Thessaloniki, Greece. In 2003, he was awarded the NATO Science Fellowship. Since May 2003 he has been a post-doctoral fellow at the Edward S. Rogers Sr. Department of Electrical and Computer Engineering at the University of Toronto in Toronto, Canada.

Dr. Lukac is a member of the IEEE Signal Processing Society. He is an active member of Review and Program Committees at various conferences and a reviewer for various scientific journals. Recently, his research interests include nonlinear digital filters, image sharpening and analysis, color image processing, CFA interpolation/zooming and digital camera image processing, image sequence processing, visual cryptography, multimedia, and the use of Boolean functions, permutation theory and artificial intelligence in filter design.

Karl Martin received the B.A.Sc. degree in Engineering Science (Electrical option) and the M.A.Sc. degree in Electrical Engineering, both at the University of Toronto, Canada in 2001 and 2003 respectively. He is currently pursuing a Ph.D. in the Edward S. Rogers Sr. Department of Electrical and Computer Engineering at the University of Toronto. His research interests include multimedia processing, wavelet-based image coding, object-based coding, and CFA processing.

Mr. Martin is a member of both the IEEE Signal Processing Society and Communications Society. Since 2003 he has been the Vice-Chair of the Signals and Applications Chapter, IEEE Toronto Section.

Konstantinos N. Plataniotis received the B. Engineering degree in Computer Engineering from the Department of Computer Engineering and Informatics, University of Patras, Patras, Greece in 1988 and the M.S and Ph.D degrees in Electrical Engineering from the Florida Institute of Technology (Florida Tech), Melbourne, Florida in 1992 and 1994 respectively. He was affiliated with the Computer Technology Institute (C.T.I), Patras, Greece from 1989 to 1991. From August 1997 to June 1999 he was an Assistant Professor with the School of Computer Science at Ryerson University. He is currently an Assistant Professor at the Edward S. Rogers Sr. Department of Electrical & Computer Engineering where he researches and teaches adaptive systems and multimedia signal processing.

Dr. Plataniotis is a Senior Member of IEEE, a past member of the IEEE Technical Committee on Neural Networks for Signal Processing, and the Technical Co-Chair of the Canadian Conference on Electrical and Computer Engineering, CCECE 2001, May 13-16, 2001, and CCECE 2004, May 2-5 2004.